Identification of S VIII through S XIV emission lines between 17.5 and 50 nm in a magnetically confined plasma

K. J. McCarthy[1], N. Tamura[2], S. K. Combs[3], R. García[1], J. Hernández Sánchez[1], M. Navarro[1], N. Panadero[1], I. Pastor[1], A. Soleto[1] and the TJ-II Team[1]

[1]Laboratorio Nacional de Fusión, CIEMAT, Madrid, Spain

[2]National Institute for Fusion Science, Toki, Japan

[3]Fusion & Materials for Nuclear Systems Division, ORNL, Tennessee, USA

author's email: kieran.mccarthy@ciemat.es

Abstract

43 spectral emission lines from F-like to Li-like sulphur ions have been identified in the wavelength range from 17.5 to 50 nm in spectra obtained following tracer injection into plasmas created in a magnetically confined plasma device, the stellarator TJ-II. Plasmas created and maintained in this heliac device with electron cyclotron resonance heating achieve central electron temperatures and densities up to 1.5 keV and 8×10^{18} m^{-3}, respectively. Tracer injections were performed with $\leq6\times10^{16}$ atoms of sulphur contained within ~300 μm diameter polystyrene capsules, termed Tracer Encapsulated Solid Pellets, using a gas propulsion system to achieve velocities between 250 and 450 m s^{-1}. Once ablation of the exterior polystyrene shell by plasma particles is completed, the sulphur is deposited in the plasma core where it is ionized up to S^{+13} and transported about the plasma. In order to aid line identification, which is made using a number of atomic line emission databases, spectra are collected before and after injection using a 1-m focal length normal incidence spectrometer equipped with a CCD camera. This work is motivated by the need to clearly identify sulphur emission lines in the vacuum ultraviolet range of magnetically confined plasmas, as sulphur X-ray emission lines are regularly observed in both tokamak and stellarator plasmas.

Keywords: Plasma, sulphur, vacuum ultraviolet, stellarator

1. Introduction

The identification of impurities (atomic elements other than fuel) in hot magnetically confined plasmas, plus the study of their origin, ionization states, and transport, is, and will continue to be, an important contribution on the pathway to the development of steady-state scenarios in fusion reactors [1, 2]. Indeed, it is well known that increasing impurity confinement at high plasma densities can lead to impurity accumulation with subsequent radiation collapse, in particular in helical devices [3]. Many impurities are intrinsically present in tokamak and stellarator plasmas [4], while other impurities are routinely injected using the gas puff, laser blow-off, dust injection, and TESPEL methods [5-8]. Hence there is a need for databases of tabulated spectral emission lines that have been clearly identified in magnetically confined plasmas. At present, there exists in the literature a limited number of spectral line surveys covering different wavelength ranges [4, 9 - 11]. In most cases such data tabulate intrinsic, vacuum wall deposited elements, and/or commonly injected elements, *e.g.*, helium, lithium, boron, carbon, nitrogen, oxygen, neon, aluminium, iron or chromium. However, other elements are often identified, albeit spectral line emissions are generally only reported for very limited wavelength ranges, *e.g.* sulphur or chlorine X-ray emission lines. Indeed, the observance of sulphur X-ray lines has been reported for many devices. For instance, when using crystal based detection systems, He-like and H-like sulphur lines were identified between 0.386 and 0.53 nm in the Alcator C tokamak [12, 13], He-like sulphur lines were observed in the Compass-D [14] and ASDEX [15] tokamaks, whilst He-like and H-like sulphur lines were observed, using a pulse height analyser system, on the recently inaugurated W7-X stellarator [16]. In all cases the source(s) of sulphur remain(s) unknown, although out-gassing tests made on anodized aluminium used in the DIII-D tokamak showed possible traces of sulphur [17]. Moreover, in the case of W7-X, an Electron Dispersive X-Ray

Spectroscopy scan of tiles from different limiters in the device revealed the presence of sulphur deposits on their surfaces [18]. Thus, sulphur is a reoccurring impurity in magnetically confined plasmas. Therefore there is a requirement to identify spectral emission lines at other wavelengths so as to broaden its database and contribute to impurity transport studies, *i.e*. to complement studies made on nearby argon. Moreover, such data can also be of interest to astrophysical community for element identification.

In this paper, trace quantities of sulphur are injected into plasmas created and maintained in the stellarator TJ-II using the tracer-encapsulated solid pellet (TESPEL) injection method [8]. TESPEL is a double-layered impurity pellet developed at the National Institute for Fusion Science in Japan. Its outer layer consists of a polystyrene $(C_8H_8)_n$ polymer while the tracer impurity is embedded in its centre that permits an impurity to be deposited within a three-dimensionally limited region in the plasma. In the TJ-II, the tracer impurity deposition occurs in the plasma core where electron temperatures are typically around 1.5 keV. Then, using a 1-m focal length normal incidence spectrometer, equipped with a CCD camera at its output focal plane, spectra are collected before and after such injections. Finally, standard spectral emission line databases allow identification of the emission lines, their ionization states and energy levels, from the injected element.

2. Experimental set-up

2.1 TJ-II stellarator

The TJ-II is a low magnetic shear stellarator of the heliac type. It has a major radius of 1.5 m with an average minor radius, a, of ≤0.22 m for its standard configuration [19]. Its magnetic fields are generated by a system of poloidal, toroidal and vertical field coils and the resultant cross-section of closed magnetic flux surfaces is bean shaped with its magnetic field at plasma centre, B_0, ≤1.1 T for the standard configuration (100-44-64 where the nomenclature reflects currents in the central, helical and vertical field coils, respectively). As a result, the

plasma volume contained within the last-closed magnetic surface (LCMS) is ~1.1 m^3. In this work, plasmas are created using hydrogen as the working gas and heated using electron cyclotron resonance heating (ECRH) with two gyrotrons operated at 53.2 GHz, *i.e.*, the 2nd harmonic of the electron cyclotron resonance frequency (P_{ECRH} ≤500 kW, $t_{discharge}$ ≤300 ms). In this way central electron densities, $N_e(0)$, and temperatures, $T_e(0)$, up to 0.7×10^{19} m^{-3} and 1.5 keV, respectively, are achieved. See Figure 1. Finally, the vacuum chamber inner walls are occasionally coated with boron and lithium, and ~30 min glow discharge cleaning with helium is performed daily, in order to improve plasma control and to reduce plasma impurity content.

2.2 TESPEL details and injections

Recently, a TESPEL injector loaned to Ciemat by the National Institute for Fusion Science at Toki, Japan was piggybacked onto the up-stream end of a cryogenic pellet injector (PI) that is operating on the TJ-II since mid-2014 [20, 21]. The PI is a 4-pellet system, developed in conjunction with the Fusion Energy Division of Oak Ridge National Laboratory, Tennessee, USA. In order to attach the TESPEL to the PI, one of the cryogenic pellet formation tubes was removed so that a vacuum-tight coupling guide tube could be attached between the TESPEL output and the up-stream end of the corresponding PI guide tube. See Figure 2. This is outlined in more detail in Ref. [21].

In TJ-II, pellets should contain $\leq 5 \times 10^{18}$ electrons for injection into ECRH plasmas in order that the post-injection central electron density does not rise above the gyrotron cut-off limit (~1.7×10^{19} m^{-3}). For this reason, ≤310 μm diameter polystyrene TESPELs, $(C_8H_8)_n$, are used for containing the tracer element. TESPELs were pre-loaded with pieces of powdered sulphur before being placed into chambers on the rotating wheel of the TESPEL injector system [8]. A good estimate of the sulphur content is established ($\leq 5 \times 10^{16}$ atoms) by measuring the dimensions of the powdered sulphur pieces to determine their volumes (a

density of 2.07 g/cm^3 is assumed [22]). Next, in order to identify spectral emission lines from hydrogen atoms and from carbon atoms or ions, empty TESPELs are also injected into reproducible plasmas. Finally, it should be noted that the laser blow-off (LBO) technique is also used on the TJ-II but the range of pure elements that can be used is limited to those that can be deposited onto quartz support slides [6].

2.3 TESPEL ablation and penetration depth

Pellet ablation in magnetically confined plasmas has been extensively studied, albeit several aspects remain to be fully understood [23]. Similarly, plasma parameter contributions to TESPEL ablation rates are known [24]. Here, plasma electrons impacting on the TESPEL outer surface ablate the polystyrene, $(C_8H_8)_n$, casing and create a cloud of neutral atoms (plasmoid) that subsequently surrounds, and travels along with, the pellet before being ionized. Optical access to the plasma, *i.e.*, through TJ-II viewports located above (TOP) and behind (SIDE) the TESPEL flight path, permits collection of the Balmer H_α light (at 656.28 nm) emitted from this cloud [20]. See Figure 2. For this, an amplified silicon diode equipped with an interference filter centred at 660 +/- 2 nm and a coherent fibre bundle is located outside the TOP viewport. Then, knowing the TESPEL velocity and its plasma entry time [21], a H_α emission profile is created and a penetration length can be established. Next, once the polystyrene casing has been fully ablated, the tracer is exposed to the plasma and incident plasma electrons stimulate light emissions from this tracer-rich plasmoid. In order to collect such light, the SIDE viewport is equipped with an avalanche photodiode (APD) and an interference filter centred on an intense neutral spectral line. Detection of this second peak confirms tracer deposition and permits its radial deposition position to be determined. Finally, the hydrogen, carbon and tracer ions trapped by the magnetic field drift along the magnetic field lines and diffuse around the plasma.

2.4 Plasma diagnostics

The TJ-II is equipped with a wide range of passive and active plasma diagnostics [25]. The principal diagnostic for this work is a 1-m normal-incidence spectrometer equipped with a 1200 grooves per mm holographic grating (aperture ratio of f/10.4) and a back-illuminated charge-coupled device (CCD) camera [26], located in a sector at 135º toroidally from the TESPEL sector. Its input slits are located 1.35 m and ~1.1 m from the plasma centre and edge, respectively. With the entrance slit width set to 50 μm, the spectral line resolution achieved is 0.0661 nm at 58.4 nm [26]. In this work, a wider entrance slit was used in order to increase light throughput. Next, spectrograms, covering a 22.5 nm wavelength range, are collected once every 3.84 ms during a plasma discharge. In order to cover a broad wavelength range, the spectrometer central wavelength at the output focal plane is moved between discharges.

Other diagnostics of interest include a single laser pulse (≤40 ns) per discharge Thomson Scattering (TS) system that provides one set of electron density and temperature profiles per discharge [27], as well as a microwave interferometer and a 12 channel Electron Cyclotron Emission (ECE) system that follow, with 10 μs temporal resolution, the line-integrated electron density and the electron temperature evolution at different radii, respectively, along a discharge [25]. These systems are located at 180º, 67.5º, and 123.75º toroidally, respectively, from the PI/TESPEL. See Figure 3. The latter microwave system provides continuous electron temperature profiles, this being essential when attempting to identify possible tracer ionization states after injection due to the large plasma temperature drop arising from the ablation process and from the addition of a population of cold TESPEL electrons ($\leq 5 \times 10^{18}$ electrons) that is similar to the plasma electron population.

3. Spectra and emission line identification

Repeated injections of individual sulphur-loaded, or unloaded, TESPELs were made into reproducible ECRH plasmas in order to compare spectra containing emission lines from

sulphur, carbon and hydrogen with spectra having emission lines from carbon and hydrogen only. Moreover, the central wavelength of the spectrometer was varied between sets of discharges in order to cover the wavelength range from 17.5 to 50 nm. This restricted wavelength range was decided beforehand due to the limited number of available sulphur-loaded TESPELs and the 50% probability of a successful injection and deposition [21]. The decision was based on criteria established during previous works in which nearby elements in the periodic table (Al, Si) were injected using LBO and TESPEL into TJ-II plasmas [4, 21]. In those cases, the observed spectral line emissions from N-like to Li-like Al and Si ions (between 28 and 60 nm) originated from transitions with upper energy levels ≤~50 eV. Using available atomic line emission databases, similar N-like to Li-like sulphur emission lines are found to occur below 50 nm [29, 30].

Spectra collected at two time instances, just before and within 20 ms after TESPEL injection, are used to produce the spectra in Figure 4. In these spectra, the identified sulphur emission lines are labelled. Numerous emission lines from highly ionized metallic elements (Fe, Cr, and Mn) that reside in the TJ-II plasma core are also identified [4]. These lines were present in the spectra before TESPEL injection. Their post-injection intensities increase due to the transitory rise in core electron density. In addition, some carbon emission lines are also identified. The source of the carbon is the C_8H_8 cladding of the TESPEL. Such lines increase immediately after an injection, (≤4 ms), but thereafter decay rapidly (≤8 ms). Next, from these spectra, the tabulated data of identified sulphur lines in Table 1 were created. It should be noted that the wavelengths are for ions at rest. With the spectrometer set-up used, Doppler wavelength displacements are significantly smaller that the spectral resolution achieved, *i.e.* 0.0661 nm at 58.4 nm [26], where poloidal and toroidal impurity ion velocities are ≤10 km/s and ≤15 km/s, respectively, for ECRH plasmas in TJ-II [31]. Moreover, in the case of poloidal velocity, the viewing solid angle collects radiation from a line-of-sight that crosses

the plasma centre (viewing +/-5 cm in the vertical direction about the plasma centre) [32]. In the case of toroidal velocity, the toroidal component of fast ions has been detected [32], but this component cannot be resolved for thermal ions. In the Table, the most intense lines of each ionization state are highlighted using a # symbol. This is done in order to aid the reader to identify spectral lines that may be suitable for plasma, or other, spectroscopic studies. In addition, unresolved close-neighbour lines from the same ion type are highlighted using an asterisk. In such cases the corresponding wavelength is the g_k x A_{ki} weighted average where g_k is the statistical weight of the upper level and A_{ki} is the transition probability [30]. From the spectra, it is seen that emission lines from F-like to Li-like sulphur are observed in TJ-II plasmas. This ionization state range is slightly broader than that found for aluminium and silicon. Moreover, several of the weaker spectral lines observed here, have upper energy levels up to 90 eV, this being somewhat higher that for aluminium and silicon (≤50 eV). This may be explained by a recent realignment of the mirrors that are closest to the plasma, in the gyrotron quasi-optical transmission lines. This has led to increased central electron temperatures, as can be seen in Figure 1 of this work and of reference [21].

4. Conclusions

Forty three spectral emission lines from F-like to Li-like sulphur ions have been identified in the stellarator TJ-II, a magnetically confined plasma device. Sulphur is an impurity element that has been regularly reported in the core of plasmas created in such devices. However, its use in impurity transport studies has been limited, rather its He-like and H-like X-ray emission lines have been used to determine electron temperatures only. One reason for this may have been the limited availability of positively identified emission lines in other wavelength and ionization stages. This has been the case for W7-X stellarator plasmas, in which sulphur X-ray emission lines were observed using a pulse height analyzer system [16] but where transport studies were limited to argon [33]. For this reason, this study should help

fill the void in the sulphur line emission database.

Acknowledgements

This work has been carried out within the framework of the EUROfusion Consortium and has received funding from the Euratom research and training programme 2014-2018 under grant agreement No 633053. The views and opinions expressed herein do not necessarily reflect those of the European Commission. In addition, it is partially financed by grants from the Spanish *Ministerio de Economía y Competitividad* (Ref. ENE2013-48679-R) and by NIFS/NINS under the project of Formation of International Scientific Base and Network (KEIN1102 and KEIN1104) and Young Researchers Supporting Program (UFEX106).

References

[1] Pospieszczyk A 2006 *Trans Fusion Sci. Tech.* **49** 395.

[2] Fujimoto T 2004 *Plasma spectroscopy* (Oxford: Oxford University Press).

[3] Burhenn R, Feng, Y, Ida K, Maassberg H, McCarthy K J, Kalinina D, Kobayashi M, Morita S, Nakamura Y, Nozato H, Okamura S, Sudo S, Suzuki C, Tamura N, Weller A, Yoshinuma M, and Zurro B 2009 Nucl. Fusion **49** 065005.

[4] McCarthy K J, Zurro B, Hollmann E M, Hernández Sánchez J and the TJ-II team 2017 Physica Scripta **57** 115601.

[5] Marmar E S, Rice J E, Terry J L and Seguin F H 1982 Nucl. Fusion **22** 1567.

[6] Zurro B, Hollmann E M, Baciero A, Ochando M A, McCarthy K J, Medina F, Velasco J L, Pastor I, Baião D, de la Cal E, Rapisarda D and TJ-II team 2014 Plasma Phys. Control. Fusion **56** 124007.

[7] Smirnov R D, Krasheninnikov S I, Pigarov A Yu, Rognilien T D, Mansfield D K, Skinner C H, and Roquemore A L 2012 Contrib. Plasma Phys **52** 435.

[8] Sudo S and Tamura N 2012 Rev. Sci. Instrum. **83** 023503.

[9] Soukhanovskii V A, McLean A G, and Allen S L 2014 Rev. Sci. Instrum. **85** 11E418.

[10] Katai R, Morita S and Goto M 2007 Plasma Fusion Res. **2** 006

[11] Machida M, Daltrini A M, Severo J H F, Nascimento I C, Sanada E K, Elizondo J I and Kuznetsov Y K 2009 Braz. J. Phys. **39** 270.

[12] Källne E and Källne J 1983 Physica Scripta **T3** 185.

[13] Källne E, Källne J and Pradhan A K 1983 Phys. Rev. A **27** 1476.

[14] Rice J E, Fournier K B, Safronova U I, Goetz J A, Gutmann S, Hubbard A E, Irby J, LaBombard B, Marmar E S, and Terry J L 1999 New J. Phys. **1** 19.

[15] Burhenn R, 1985, Dissertation, Ruhr-Universität Bochum, Institut für Experimentalphysik V.

[16] Krawczyk N, Biedermann C, Czarnecka A, Fornal T, Jablonski S, Kaczmarczyk J, Kubkowska M, Kunkel F, McCarthy K J, Ryć L, Thomsen H, Weller A and W7-X team 2017 Fusion. Eng. Design **123** 1006.

[17] Holtrop K L and Hansink K J 2006 J. Vac Sci. Tech. A **24** 1572.

[18] Winters V R, Brezinsek S, Effenberg F, Rasinski M, Schmitz O, Stephey L, Biedermann C, Dhard C P, Frerichs H, harris J, Kjychowiak M, König R, Sunn Pedersen T, Wurden G A and W7-X team 2017 Physica Scripta **T170** 014050.

[19] Sánchez J, *et al*. 2015 Nucl. Fusion **55** 104014.

[20] McCarthy K J, Panadero N, Arapoglou I, Combs S K, Caughman J B O, de la Cal E, Foust C, García R, Hérnandez-Sánchez J, Martín F, Navarro M, Ochando M A, Pastor I, Rodríguez M C and Velasco J L 2015 1st EPS Conf. on Plasma Diagnostics, Proc.of Science (ECPD) (Frascati, Italy, 2015).

[21] Tamura N, McCarthy K J, Hayashi H, Combs S K, Foust C, García R, Panadero N, Pawelec E, Hernández Sánchez J, Navarro M, Soleto A and TJ-II team, 2016 Rev. Sci. Instrum. **87** 11D619.

[22] Lide D R, 1991-1992 *CRC Handbook of Chemistry and Physics 72nd Edition* (Boca Raton: CRC Press Incorporated).

[23] Pégourié B 2007 Plasma Phys. Control. Fusion **49** R87.

[24] Khlopenkov K V and Sudo S, 1998 Rev. Sci. Instrum. **69** 3196.

[25] McCarthy K J *Diagnostic tools for probing hot magnetically confined plasmas*, XXXIII Reunión Bienal de la Real Sociedad Española de Física: 21er Encuentro Ibérico para la Enseñanza de la Física: PUBliCan, ediciones de la Universidad de Cantabria, Santander, Spain, **IV** (2011) 65. ISBN 978-84-86116-40-8.

[26] McCarthy K J, Zurro B, Balbín R, Baciero A, Herranz J, and Pastor I 2003 Europhys. Lett. **63** 49.

[27] Herranz J, Castejón F, Pastor I and McCarthy K J 2003 Fusion Eng. Des. **65** 525.

[28] McCarthy K J, Panadero N, Velasco J L, Combs S K, Caughman J B O, Fontdecaba J M, Foust C, García R, Hernández Sánchez J, Navarro M, Pastor I, Soleto A and TJ-II team

(2017) Nucl. Fusion **57** 056039.

[29] Kramida K, Ralchenko Yu, and Reader J NIST ASD Team 2015. *NIST Atomic Spectra Database* (Gaithersburg, MD: national Institute of Standards and Technology) (version 5.3), [Online]. Available: http://physics.nist.gov/asd [25 June 2017]

[30] The Atomic Line List V2.05B19 at (http://www.pa.uky.edu/~peter/newpage/).

[31] Arévalo J, Alonso J A, McCarthy K J and Velasco J L 2013 Nucl. Fusion **53** 023003.

[32] McCarthy K J, Tribaldos V, Arévlo J, and Liniers M 2010 J. Phys. B: At. Mol. Opt. Phys. **43** 144020.

[33] Langenberg A, Pablant N A, Marchuk O, Zhang D, Alonso J A, Burhenn R, Svensson J, Valson P, Gates D, Beurskens M, Wolf R C, and W7-X team 2017 Nucl. Fusion **57** 086013.

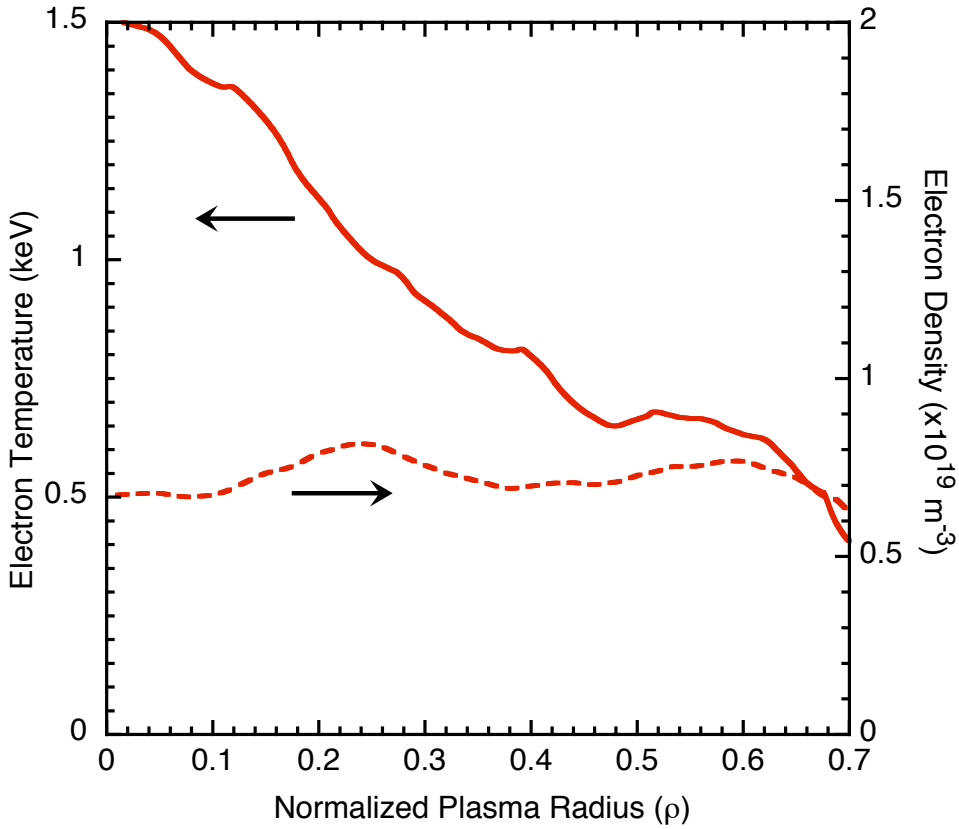

Figure 1: Electron temperature (continuous) and density (dashed) profiles of the target plasmas used in this study. These were obtained using the Thomson Scattering Diagnostic which is limited to measurements within $\rho \leq 0.7$.

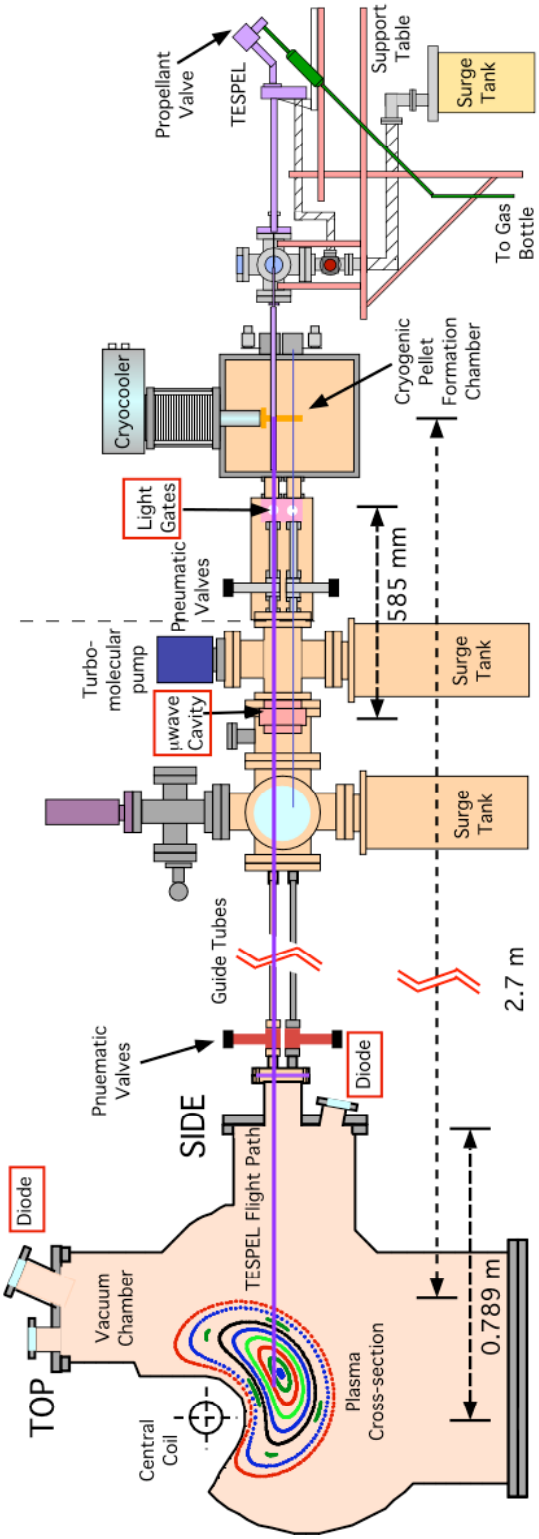

Figure 2: Sketch showing a cross-section of the vacuum chamber of the stellarator TJ-II, the cryogenic pellet injector (PI) and the TESPEL injector connected to the up-stream end of the PI. The locations of the TOP and SIDE viewports, and the light diodes are highlighted.

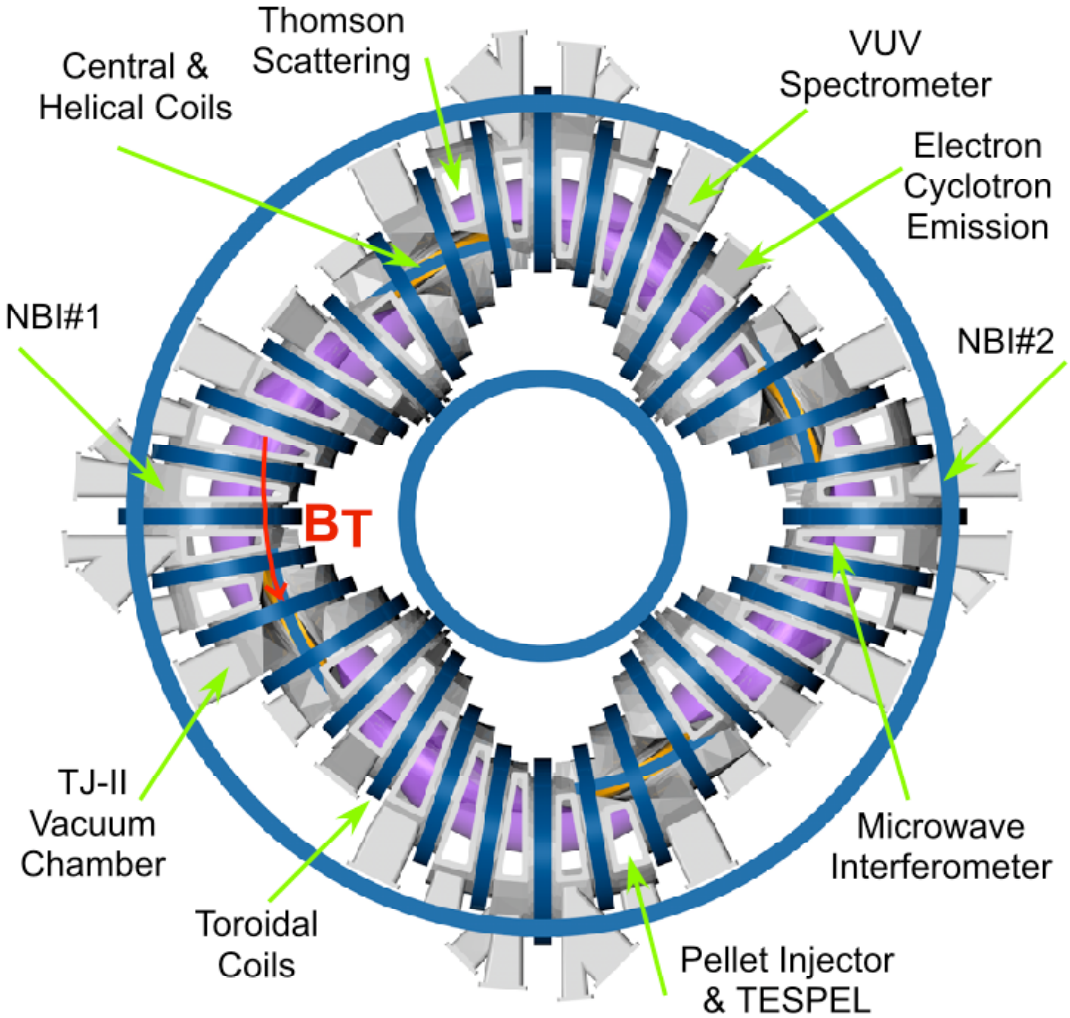

Figure 3: Bird's eye view of the stellarator TJ-II. The locations of the Pellet Injector/TESPEL system and the VUV spectrometer, as well as its principal components are highlighted [28].

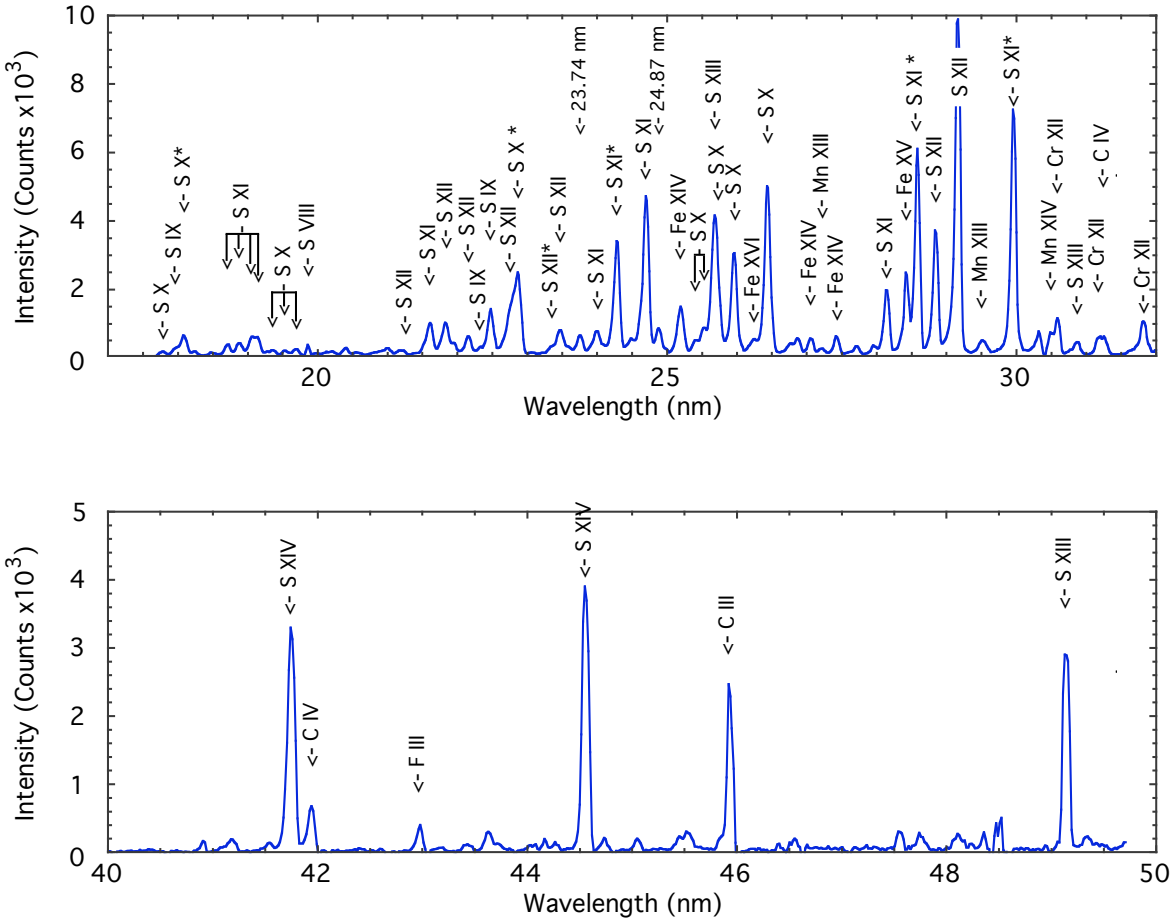

Figure 4. Spectra showing the sulphur lines identified after sulphur-loaded TESPEL injections into TJ-II plasmas. Each spectrum is the difference between spectra collected before and after an injection. Note: the spectrometer sensitivity drops off rapidly at the shortest wavelengths (below ~20 nm). Relatively intense emission lines from other ions in TJ-II are also identified [4]. The authors have been unable to positively identify the emission lines in the spectrum at 23.74 nm and 24.87 m from the spectral line databases consulted [28, 29]. Although some S and C candidates exist, it is found, after comparison, that either their upper energy level, ionization state, or A_{ki} do not concur with those of identified S and C lines.

Wavelength (nm)	Ion	Notation	Transition
17.755	S^{+9}	S X	$2s^22p^3\ ^2D^0$ - $2s2p^4\ ^2P$
17.929	S^{+8}	S IX	$2s^22p^4\ ^1D$ - $2s2p^5\ ^1P^0$
18.067*	S^{+9}	S X	$2s^22p^3\ ^2D^0$ - $2s2p^4\ ^2P$
18.684	S^{+10}	S XI	$2s2p^2\ ^3P$ - $2s2p^3\ ^3S^0$
18.868	S^{+10}	S XI	$2s2p^2\ ^3P$ - $2s2p^3\ ^3S^0$
19.036	S^{+10}	S XI	$2s2p^2\ ^3P$ - $2s2p^3\ ^3S^0$
19.126	S^{+10}	S XI	$2s2p^2\ ^3P$ - $2s2p^3\ ^3S^0$
19.349	S^{+9}	S X	$2s^22p^3\ ^2P^0$ - $2s2p^4\ ^2P$
19.612	S^{+9}	S X	$2s^22p^3\ ^2P^0$ - $2s2p^4\ ^2P$
19.682	S^{+9}	S X	$2s^22p^3\ ^2P^0$ - $2s2p^4\ ^2P$
19.855#	S^{+7}	S VIII	$2s^22p^5\ ^2P^0$ - $2s2p^6\ ^2S$
20.755	S^{+9}	S X	$2s^22p^3\ ^2P^0$ - $2s2p^4\ ^2S$
20.7967	S^{+11}	S XII	$2s^22p\ ^2P^0$ - $2s2p^2\ ^2P$
20.834	S^{+9}	S X	$2s^22p^3\ ^2P^0$ - $2s2p^4\ ^2S$
21.212	S^{+11}	S XII	$2s^22p\ ^2P^0$ - $2s2p^2\ ^2P$
21.517	S^{+11}	S XII	$2s^22p\ ^2P^0$ - $2s2p^2\ ^2P$
21.5968	S^{+10}	S XI	$2s^22p^2\ ^1D$ - $2s2p^3\ ^1D^0$
21.821	S^{+11}	S XII	$2s^22p\ ^2P^0$ - $2s2p^2\ ^2P$
22.124	S^{+8}	S IX	$2s^22p^4\ ^3P$ - $2s2p^5\ ^3P^0$
22.143	S^{+11}	S XII	$2s^22p\ ^2P^0$ - $2s2p^2\ ^2P$
22.329	S^{+8}	S IX	$2s^22p^4\ ^3P$ - $2s2p^5\ ^3P^0$
22.477#	S^{+8}	S IX	$2s^22p^4\ ^3P$ - $2s2p^5\ ^3P^0$
22.75	S^{+11}	S XII	$2s^22p\ ^2P^0$ - $2s2p^2\ ^2S$
22.8476*	S^{+9}	S X	$2s^22p^3\ ^2D^0$ - $2s2p^4\ ^2D$
23.348*	S^{+11}	S XII	$2s^22p\ ^2D$ - $2p^3\ ^2P^0$
23.448	S^{+11}	S XII	$2s^22p\ ^2P^0$ - $2s2p^2\ ^2S$
23.982	S^{+10}	S XI	$2s^22p^2\ ^3P$ - $2s2p^3\ ^3P^0$
24.278*	S^{+10}	S XI	$2s^22p^2\ ^3P$ - $2s2p^3\ ^3P^0$

24.689	S^{+10}	S XI	$2s^22p^2\ ^3P$ - $2s2p^3\ ^3P^0$
25.397	S^{+9}	S X	$2s^22p^3\ ^2P^0$ - $2s2p^4\ ^2D$
25.5063	S^{+9}	S X	$2s^22p^3\ ^2P^0$ - $2s2p^4\ ^2D$
25.668#	S^{+12}	S XIII	$1s^22s^2\ ^1S$ - $1s^22s2p\ ^1P^0$
25.714	S^{+9}	S X	$2s^22p^3\ ^4P^0$ - $2s2p^4\ ^4P$
25.95	S^{+9}	S X	$2s^22p^3\ ^4S^0$ - $2s2p^4\ ^4P$
26.424#	S^{+9}	S X	$2s^22p^3\ ^4S^0$ - $2s2p^4\ ^4P$
28.14	S^{+10}	S XI	$2s^22p^2\ ^3P$ - $2s2p^3\ ^3D^0$
28.5777*	S^{+10}	S XI	$2s^22p^2\ ^3P$ - $2s2p^3\ ^3D^0$
28.8416	S^{+11}	S XII	$2s^22p\ ^2P^0$ - $2s2p^2\ ^2D$
29.158#	S^{+10}	S XI	$2s^22p^2\ ^3P$ - $2s2p^3\ ^3D^0$
29.9536#	S^{+11}	S XII	$2s^22p\ ^2P^0$ - $2s2p^2\ ^2D$
30.894	S^{+12}	S XIII	$1s^22s2p\ ^3P^0$ - $1s^22p^2\ ^3P$
41.766	S^{+13}	S XIV	$1s^22s\ ^2S$ - $1s^22p\ ^2P^0$
44.57#	S^{+13}	S XIV	$1s^22s\ ^2S$ - $1s^22p\ ^2P^0$
49.146#	S^{+12}	S XIII	$1s^22s^2\ ^1S$ - $1s^22s2p\ ^3P^0$

Table I: List of identified sulphur emission lines in TJ-II plasmas after sulphur loaded TESPEL injection together with the emitting ions, their spectroscopic notation and the identified transition. Here, the symbol # identifies the most intense line of each ionization state while the symbol * signifies g_k x A_{ki} weighted average wavelengths for unresolved lines emitted by the same ion.